The effect of growth sequence on magnetization damping in Ta/CoFeB/MgO structures

Bo Liu,[a†] Dawei Huang,[a†] Ming Gao,[a] Hongqing Tu,[b] Kejie Wang,[a] Xuezhong Ruan,[a,*] Jun Du,[b] Jian-Wang Cai,[c,*] Liang He,[a] Jing Wu,[d] Xinran Wang,[a] and Yongbing Xu[a,d,*]

[a]Jiangsu Provincial Key Laboratory of Nanotechnology, Collaborative Innovation Center of Advanced Microstructures, School of Electronic Science and Engineering, Nanjing University, Nanjing 210093, People's Republic of China

[b]Department of Physics, Nanjing University, Nanjing 210093, People's Republic of China

[c]Beijing National Laboratory for Condensed Matter Physics, Institute of Physics, Chinese Academy of Sciences

[d]York-Nanjing International Center in Spintronics (YNICS), Department of Electronics and Physics, The University of York, York YO10 5DD, UK

E-mail: xzruan@nju.edu.cn, jwcai@aphy.iphy.ac.cn and ybxu@nju.edu.cn

Abstract:

Magnetization damping is a key parameter to control the critical current and the switching speed in magnetic random access memory, and here we report the effect of the growth sequence on the magnetic dynamics properties of perpendicularly magnetized Ta/CoFeB/MgO structures. Ultrathin CoFeB films have been grown between Ta and MgO but with different stack sequences, i.e. substrate/Ta/CoFeB/MgO/Ta and substrate/Ta/MgO/CoFeB/Ta. The magnetization dynamics induced by femtosecond laser was investigated by using all-optical pump-probe measurements. We found that the Gilbert damping constant was modulated by reversing stack structures, which offers the potential to tune the damping parameter by the growth sequence. The Gilbert damping constant was enhanced from 0.017 for substrate/Ta/CoFeB/MgO/Ta to 0.027 for substrate/Ta/MgO/CoFeB/Ta. We believe that this enhancement originates from the increase of intermixing at the CoFeB/Ta when the Ta atom layer was grown after the CoFeB layer.

1. Introduction

Current-induced spin-transfer torque (STT) is very important in high density magnetic media and spintronics devices[1-5]. Regarding the energy consumption, it is critcal to find out the method to reduce the critical current that switches the spin direction in STT-MRAM application. According to S. Mangin et al[6], the current density J_{C0} is proportional to the Gilbert damping constant α and effective magnetic

anisotropic energy K_u^{eff}. Therefore, either decreasing the damping values or magnetic anisotropy energy is required to reduce the critical current. However, considering the thermal stability of the MTJ devices, we cannot decrease the anisotropy energy too much. Thus, it is a better choice to reduce the damping constant and at the same time, relatively high magnetic anisotropy energy is preferable. The high perpendicular magnetic anisotropy materials such as L10-FePt and Co/Pt multilayers[7-10] that are integrated into the magnetic tunnel junction (MTJ) [11,12] are reported to both have low damping constant and relative high thermal stability. These materials are found to be in the good balance of thermal stability and low damping constant. The optimization of the Gilbert damping constant α is critial to achieve a higher thermal stability and a lower threshold current density [13]. A major breakthrough in MRAM is the discovery of the perpendicularly magnetized CoFeB films sandwiched by MgO and Ta layers, which exhibit not only perpendicular magnetic anisotropy, but also moderate magnetic damping constant[14,15].

In this paper, we report the effect of the stack growth sequence on the Gilbert damping constants in the Ta/CoFeB/MgO structures grown by sputtering. A time-resolved optical pump-probe technique was used to investigate the precessional dynamics and the magnetization damping. We have observed a remarkable difference of the damping constants between the samples grown with different stack sequences. The experimental results clearly demonstrate that stack growth sequence plays a key role in controlling damping values. .

2. Methods

We prepared two sets of samples: substrate/Ta (5)/CoFeB (1)/MgO (3)/Ta (5) named as sample A and substrate/Ta (5)/MgO (3)/CoFeB (1)/Ta (5) named as sample B (numbers are thickness in nanometers). The capping layer and $Co_{40}Fe_{40}B_{20}$ films were deposited on Si (001)/SiO$_2$ substrates by dc sputtering, whereas the MgO layer was deposited by rf sputtering. The background vacuum was about 4×10^{-5} Pa and the working argon pressure was 0.5 Pa. After the thin film was deposited, a post-annealing process at 300 °C in vacuum (4×10^{-5} Pa) was performed for half an hour on both of the samples. Static magnetic properties were obtained by using a vibrating sample magnetometer(VSM). The surface morphology and roughness were analyzed by atomic force microscopy (AFM). The femtosecond pulse train generated by a Ti: sapphire laser with a pulse duration of 50 fs and a repetition rate of 1 kHz was divided into pump and probe pulse beam. The pump pulse beam with a fluence of 3.54 mJ/cm^2 was focused to a spot of ~600 μm in diameter on the sample to excite the magnetization precession, while the probe pulse beam with a fluence of 0.06 mJ/cm^2 was focused to a spot size of ~200 μm in diameter and overlapped with the pump laser spot on the sample surface [16-20]. The Kerr rotation of reflected probe pulse beam was detected by a balanced detector. A mechanical delay line was used to generate time delay between pump and probe pulse beams. The magnetization dynamics was studied by time-resolved magneto-optical Kerr effect (TRMOKE) measurements. A variable magnetic field was applied at an angle of 30° from the sample plane resulting in a cant of the magnetization away from the normal of the

film. All presented results were obtained at room temperature unless otherwise specified.

3. Results and discussion

The magnetic hysteresis loops of sample A and sample B were measured with the in-plane and perpendicular magnetic fields using VSM and displayed in Fig. 1(a) and (b), respectively. The results display a similar coercivity (H_c) and saturation magnetization (M_s) between two samples with $H_c = 5.31$ Oe and $M_s = 890$ emu/cm^3 for sample A, $H_c = 5.66$ Oe and $M_s = 836$ emu/cm^3 for sample B. The Hc is defined along the easy axis that is out-of-plane [21-23].

The AFM images of the sample A and sample B are shown in Fig. 2(a) and (b), respectively. The root-mean-square (RMS) of the surface roughness is about 0.83 nm for sample A and about 1.11 nm for sample B, respectively, which suggests that the underlayer Ta below CoFeB in sample A might lead to a reduction of the surface roughness. However, we found little difference of the K_u^{eff} defined by $H_k M_s/2$ between two samples with 1.24 Merg/cm^3 for sample A and 1.25 Merg/cm^3 for sample B, which suggests that the surface roughness has not changed dramatically the static magnetic properties, such as the saturation magnetization and the effective anisotropy field. More specifically, the effective anisotropy field here mainly arises from the interfacial perpendicular anisotropy[8].

In pump-probe measurements, the pump laser pulse created a thermal excitation of the electron/spin system leading to an ultrafast demagnetization. The magnetic

order started to recover as electron/spin-transferred energy to lattice and reached a new electron/lattice/spin equilibrium within a few picoseconds. As the heat further diffused into the surrounding area and down to the substrate, the magnetization was partially recovered. Following the recovery of the magnetization, the magnetic anisotropy was also recovered, leading to a rise of anisotropy field along the direction perpendicular to the sample plane in a time period of tens of picoseconds. Then, the magnetization precessed around the initial equilibrium direction of effective field. Fig. 3(a) shows the geometry diagram of our TRMOKE measurements, and Fig. 3(b), (c) show typical TRMOKE curves for the sample A and sample B, respectively. The signals were measured at different external magnetic fields (H_{ext}) with a fixed field angle $\theta_H = 60°$, which is the angle between the normal direction of sample plane and the external magnetic field. The data can be analyzed using an exponential damped sinusoide [16,24-26],

$$\theta_k = Aexp(-vt) + Bexp(-t/\tau)\,sin(2\pi ft + \varphi) \tag{1}$$

the first term is an approximate expression for recovery from ultrafast demagnetization observed as a slowly changing background; A are amplitudes, and v is the recovery rate of magnetization. The second term corresponds to the damped magnetization precession; B, τ, f, and φ are amplitude, relaxation time, frequency, and the initial phase of magnetization precession, respectively[17,27]. From a fit to the Kerr rotation spectra, we extracted the values of the τ and f.

As shown in Fig. 4(a) and (b), f and $1/\tau$ are plotted as functions of H_{ext} for the sample A and sample B. The f can be reproduced well by the dispersion

equation $2\pi f = \gamma(H_1 H_2)^{1/2}$, where $H_1 = H\cos(\theta_H - \theta) + H_K(\cos\theta)^2$, $H_2 = H\cos(\theta_H - \theta) + H_K \cos 2\theta$, $H_K = 2K_u/M_S - 4\pi M_S$ with uniaxial anisotropy constant K_u, gyromagnetic ratio γ, and $\theta_H = 60°${Mizukami: 2008jp}, The equilibrium angular position θ of the magnetization satisfies the function $\sin 2\theta = (2H/H_K)\sin(\theta_H - \theta)$. By this analysis procedure, the obtained fitted parameters H_k for sample A and B are 0.87 and 0.96 KOe, respectively. The fitted values are a little less than the measured effective anisotropy filed from the VSM measurement as shown in Fig.1 (a) and (b). This may originate from the small remanence along the in-plane direction. For each sample, an approximately linear increase in the oscillation frequency is observed at high applied magnetic field. When the applied field is reduced, a deviation from this linear behavior is seen because the anisotropy field contributes to the frequency and the damping becomes much more obvious. The magnetization relaxation rate $1/\tau$ fluctuates around a constant in sample A, whereas decreases considerably in sample B as the external magnetic field increases. This may be related to electron-impurity interaction dominating the scattering events caused by structural imperfections on the CoFeB/Ta interface[10,28].

We calculate the effective Gilbert damping constant by the formula $\alpha_{eff} = 1/2\pi f\tau$, which includes the intrinsic Gilbert damping constant α and the extrinsic contribution. The dependences of α_{eff} are plotted in Fig. 4(c). For the sample A and sample B, in the low field regime α_{eff} is large and decreases continuously with increasing the magnetic field. While in the high field regime, it varies gently and nearly reaches a constant. The undesirable dephasing and inhomogeneous anisotropy

distribution are suppressed under a strong external field so that the precession is closer to a coherent macro-spin mode, and thus the damping constants at high field represent the intrinsic Gilbert damping constant. As shown clearly in the inset of Fig. 4(c), the intrinsic Gilbert damping constant α is approximately 0.017 for sample A, and 0.027 for sample B. For the given thickness at around 1nm within the Ta/CoFeB/MgO sample structure, the damping constants obtained in our results are consistent with previous reports[3,29,30].It is also reported by G. Malinowski et al that the damping values of PMA CoFeB were about 10 times higher than ours when the thickness was within 0.45-0.65nm.

The enhancement of α for ferro/nonmagnetic interfaces by spin pumping was discussed theoretically by Tserkovnyak et al, and the level of enhancement α' was expressed as[31],

$$\alpha' = (\hbar\gamma/2\pi M_s)(g^{\uparrow\downarrow}S^{-1}/t_{CoFeB}) \qquad (2)$$

where $g^{\uparrow\downarrow}$ and S^{-1} denote the mixing conductance and the cross-section area, respectively. When sputtered on top of CoFeB, the Ta layer might intermix with the CoFeB because the Ta is a heavy metal and has a higher kinetic energy emitted from the target. At the same time, the boron atoms diffuse out from the CoFeB layer and are absorbed easily by Ta layer during annealing[8,28,32,33]. Considering the equation (2), we believe that the B and Ta atoms cause α to increase by the increase of the mixing conductance in the CoFeB/Ta interface. Meanwhile, according to the Elliott-Yafet relaxation mechanism, the magnetization damping experiences a substantial increase when B and Ta atoms are inside CoFe, originating from a scatter

of electrons [34,35]. Recently, it was demonstrated that the MgO interface suppresses the spin-pumping effect in MgO/FeB/MgO/Ta structures[4,36], and the CoFeB/Ta interface plays an important role in enhancing the α [37]. This means that α' of the CoFeB/MgO interface is negligibly small when compared with that of the CoFeB/Ta interface. Our work here demonstrates that the growth sequence of the CoFeB/Ta interface can further modulate the magnetic dynamic properties.

4. Conclusion

In conclusion, we investigated the ultrafast magnetization precession in perpendicularly magnetized substrate/Ta/CoFeB/MgO/Ta and substrate/Ta/MgO/CoFeB/Ta films by all optical TRMOKE measurements. The Gilbert damping constant in these two sample structures shows clearly difference by reversing the capping layer and the underlayer, which is related to the increase of the mixing conductance in the interface of CoFeB/Ta induced by B and Ta atoms. While the static magnetic properties are largely unchanged, the magnetization damping depends sensitively on the growth sequence of the CoFeB/Ta interface, which provides a new approach to tune the critical current in the MRAM. According to our findings, the growth sequence of the MRAM stacks is of great importance in changing the damping constants and therefore controlling the critical current in the application of MRAM.

References

[1]   J. Sinha, M. Gruber, M. Kodzuka, T. Ohkubo, S. Mitani, K. Hono, et al., Influence of boron diffusion on the perpendicular magnetic anisotropy in Ta vertical bar CoFeB vertical bar MgO ultrathin films, Journal of Applied Physics. 117 (2015). doi:10.1063/1.4906096.

[2]   D. Kim, K.Y. Jung, S. Joo, Y. Jang, J. Hong, B.C. Lee, et al., Perpendicular magnetization of CoFeB on top of an amorphous buffer layer, Journal of Magnetism and Magnetic Materials. 374 (2015) 350–353. doi:10.1016/j.jmmm.2014.08.030.

[3]   S. Iihama, S. Mizukami, H. Naganuma, M. Oogane, Y. Ando, T. Miyazaki, Gilbert damping constants of Ta/CoFeB/MgO(Ta) thin films measured by optical detection of precessional magnetization dynamics, Phys Rev B. 89 (2014) 174416. doi:10.1103/PhysRevB.89.174416.

[4]   X. Liu, W. Zhang, M.J. Carter, G. Xiao, Ferromagnetic resonance and damping properties of CoFeB thin films as free layers in MgO-based magnetic tunnel junctions, Journal of Applied Physics. 110 (2011) 033910–6. doi:10.1063/1.3615961.

[5]   Q. Zhang, L. You, X. Shen, C. Wan, Z. Yuan, X. Zhang, et al., Polarization-Mediated Thermal Stability of Metal/Oxide Heterointerface, Advanced Materials. 27 (2015) 6934–6938. doi:10.1002/adma.201502754.

[6]   S. Mangin, D. Ravelosona, J.A. Katine, M.J. Carey, B.D. Terris, E.E. Fullerton, Current-induced magnetization reversal in nanopillars with perpendicular anisotropy, Nat Mater. 5 (2006) 210–215. doi:10.1038/nmat1595.

[7]   T. Zhu, Anomalous Hall effect in perpendicular CoFeB thin films, Chinese Physics B. 23 (2014) 047504. doi:10.1088/1674-1056/23/4/047504.

[8]   S. Ikeda, K. Miura, H. Yamamoto, K. Mizunuma, H.D. Gan, M. Endo, et al., A perpendicular-anisotropy CoFeB–MgO magnetic tunnel junction, Nat Mater. 9 (2010) 721–724.

[9]   A. Brataas, A.D. Kent, H. Ohno, Current-induced torques in magnetic materials, Nat Mater. 11 (2AD) 372.

[10]   T. Zhu, Y. Yang, R.C. Yu, H. Ambaye, V. Lauter, J.Q. Xiao, The study of perpendicular magnetic anisotropy in CoFeB sandwiched by MgO and tantalum layers using polarized neutron reflectometry, Appl. Phys. Lett. 100 (2012) 202406. doi:10.1063/1.4718423.

[11]   M. Yoshikawa, E. Kitagawa, T. Nagase, T. Daibou, M. Nagamine, K. Nishiyama, et al., IEEE Transactions on Magnetics. 44 (n.d.) 2573 –2576.

[12] K. Mizunuma, S. Ikeda, J.H. Park, H. Yamamoto, H. Gan, K. Miura, et al., MgO barrier-perpendicular magnetic tunnel junctions with CoFe/Pd multilayers and ferromagnetic insertion layers, Appl. Phys. Lett. 95 (2009) 232516. doi:10.1063/1.3265740.

[13] S. Mizukami, Fast Magnetization Precession and Damping for Magnetic Films with High Perpendicular Magnetic Anisotropy, J. Magn. Soc. Jpn. 39 (2015) 1–7. doi:10.3379/msjmag.1412R001.

[14] T. Liu, Y. Zhang, J.W. Cai, H.Y. Pan, Thermally robust Mo/CoFeB/MgO trilayers with strong perpendicular magnetic anisotropy, Scientific Reports. 4 (2AD) 5895.

[15] E. Barati, M. Cinal, D.M. Edwards, A. Umerski, Gilbert damping in magnetic layered systems, Phys Rev B. 90 (2014) 014420. doi:10.1103/PhysRevB.90.014420.

[16] H.-S. Song, K.-D. Lee, J.-W. Sohn, S.-H. Yang, S.S.P. Parkin, C.-Y. You, et al., Observation of the intrinsic Gilbert damping constant in Co/Ni multilayers independent of the stack number with perpendicular anisotropy, Appl. Phys. Lett. 102 (2013) 102401. doi:10.1063/1.4795013.

[17] X. Ma, L. Ma, P. He, H.B. Zhao, S.M. Zhou, G. L upke, Role of antisite disorder on intrinsic Gilbert damping in $L1_0$ FePt films, Phys Rev B. 91 (2015) 014438. doi:10.1103/PhysRevB.91.014438.

[18] W. He, B. Hu, Q.-F. Zhan, X.-Q. Zhang, Z.-H. Cheng, Probing nonlinear magnetization dynamics in Fe/MgO(001) film by all optical pump-probe technique, Appl. Phys. Lett. 104 (2014) 142405. doi:10.1063/1.4871006.

[19] A. Ganguly, R.M. Rowan-Robinson, A. Haldar, S. Jaiswal, J. Sinha, A.T. Hindmarch, et al., Time-domain detection of current controlled magnetization damping in Pt/Ni81Fe19 bilayer and determination of Pt spin Hall angle, Appl. Phys. Lett. 105 (2014) 112409. doi:10.1063/1.4896277.

[20] G. Woltersdorf, M. Buess, B. Heinrich, C.H. Back, Time Resolved Magnetization Dynamics of Ultrathin Fe(001) Films: Spin-Pumping and Two-Magnon Scattering, Phys. Rev. Lett. 95 (2005) 037401. doi:10.1103/PhysRevLett.95.037401.

[21] Y.S. Chen, C.-W. Cheng, G. Chern, W.F. Wu, J.G. Lin, Ferromagnetic resonance probed annealing effects on magnetic anisotropy of perpendicular CoFeB/MgO bilayer, Journal of Applied Physics. 111 (2012) 07C101. doi:10.1063/1.3670042.

[22] J.W. Koo, S. Mitani, T.T. Sasaki, H. Sukegawa, Z.C. Wen, T. Ohkubo, et al., Large perpendicular magnetic anisotropy at Fe/MgO interface, Appl. Phys. Lett. 103 (2013) 192401. doi:10.1063/1.4828658.

[23] J. Okabayashi, J.W. Koo, H. Sukegawa, S. Mitani, Y. Takagi, T. Yokoyama, Perpendicular magnetic anisotropy at the interface between ultrathin Fe film and MgO studied by angular-dependent x-ray magnetic circular dichroism, Appl. Phys. Lett. 105 (2014) 122408. doi:10.1063/1.4896290.

[24] P. He, X. Ma, J.W. Zhang, H.B. Zhao, G. Lupke, Z. Shi, et al., Quadratic scaling of intrinsic Gilbert damping with spin-orbital coupling in L10 FePdPt

films: experiments and Ab initio calculations, Phys. Rev. Lett. 110 (2013) 077203. doi:10.1103/PhysRevLett.110.077203.

[25] S. Qiao, S. Nie, J. Zhao, X. Zhang, The thickness-dependent dynamic magnetic property of Co 2FeAl films grown by molecular beam epitaxy, Appl. Phys. Lett. 105 (2014) 172406. doi:10.1063/1.4900792.

[26] G. Malinowski, K.C. Kuiper, R. Lavrijsen, H. Swagten, B. Koopmans, Magnetization dynamics and Gilbert damping in ultrathin Co48Fe32B20 films with out-of-plane anisotropy, Appl. Phys. Lett. 94 (2009) 102501.

[27] Z. Wen, H. Sukegawa, T. Furubayashi, J. Koo, K. Inomata, S. Mitani, et al., A 4-Fold-Symmetry Hexagonal Ruthenium for Magnetic Heterostructures Exhibiting Enhanced Perpendicular Magnetic Anisotropy and Tunnel Magnetoresistance, Advanced Materials. 26 (2014) 6483–6490. doi:10.1002/adma.201401959.

[28] W.X. Wang, Y. Yang, H. Naganuma, Y. Ando, R.C. Yu, X.F. Han, The perpendicular anisotropy of Co 40Fe 40B 20sandwiched between Ta and MgO layers and its application in CoFeB/MgO/CoFeB tunnel junction, Appl. Phys. Lett. 99 (2011) 012502. doi:10.1063/1.3605564.

[29] S. Iihama, Q.L. Ma, T. Kubota, S. Mizukami, Y. Ando, T. Miyazaki, Damping of Magnetization Precession in Perpendicularly Magnetized CoFeB Alloy Thin Films, Appl Phys Express. 5 (2012) 083001. doi:10.1143/Apex.5.083001.

[30] A. Conca, E.T. Papaioannou, S. Klingler, J. Greser, T. Sebastian, B. Leven, et al., Annealing influence on the Gilbert damping parameter and the exchange constant of CoFeB thin films, Appl. Phys. Lett. 104 (2014) 182407.

[31] Y. Tserkovnyak, A. Brataas, G.E.W. Bauer, Spin pumping and magnetization dynamics in metallic multilayers, Phys Rev B. 66 (2002) 224403. doi:10.1103/PhysRevB.66.224403.

[32] J. Sinha, M. Gruber, M. Kodzuka, T. Ohkubo, S. Mitani, K. Hono, et al., Influence of boron diffusion on the perpendicular magnetic anisotropy in Ta vertical bar CoFeB vertical bar MgO ultrathin films, Journal of Applied Physics. 117 (2015) 043913. doi:10.1063/1.4906096.

[33] J.-W. Sohn, H.-S. Song, J.-W. Kim, I.-J. Shin, B.-C. Min, C.-Y. You, et al., Gilbert damping in asymmetric MgO(Ta)/CoFeB/Ta(MgO) structures with perpendicular magnetic anisotropy, Current Applied Physics. 16 (2016) 481–485. doi:http://dx.doi.org/10.1016/j.cap.2015.12.002.

[34] R.J. Elliott, Theory of the Effect of Spin-Orbit Coupling on Magnetic Resonance in Some Semiconductors, Phys Rev. 96 (1954) 266–279. doi:10.1103/PhysRev.96.266.

[35] V. Kamberský, On the Landau–Lifshitz relaxation in ferromagnetic metals, Can. J. Phys. 48 (1970) 2906–2911. doi:10.1139/p70-361.

[36] S. Mizukami, Y. Ando, T. Miyazaki, Effect of spin diffusion on Gilbert damping for a very thin permalloy layer in Cu/permalloy/Cu/Pt films, Phys Rev B. 66 (2002) 104413. doi:10.1103/PhysRevB.66.104413.

[37] A. Natarajarathinam, Z.R. Tadisina, T. Mewes, S. Watts, E. Chen, S. Gupta,
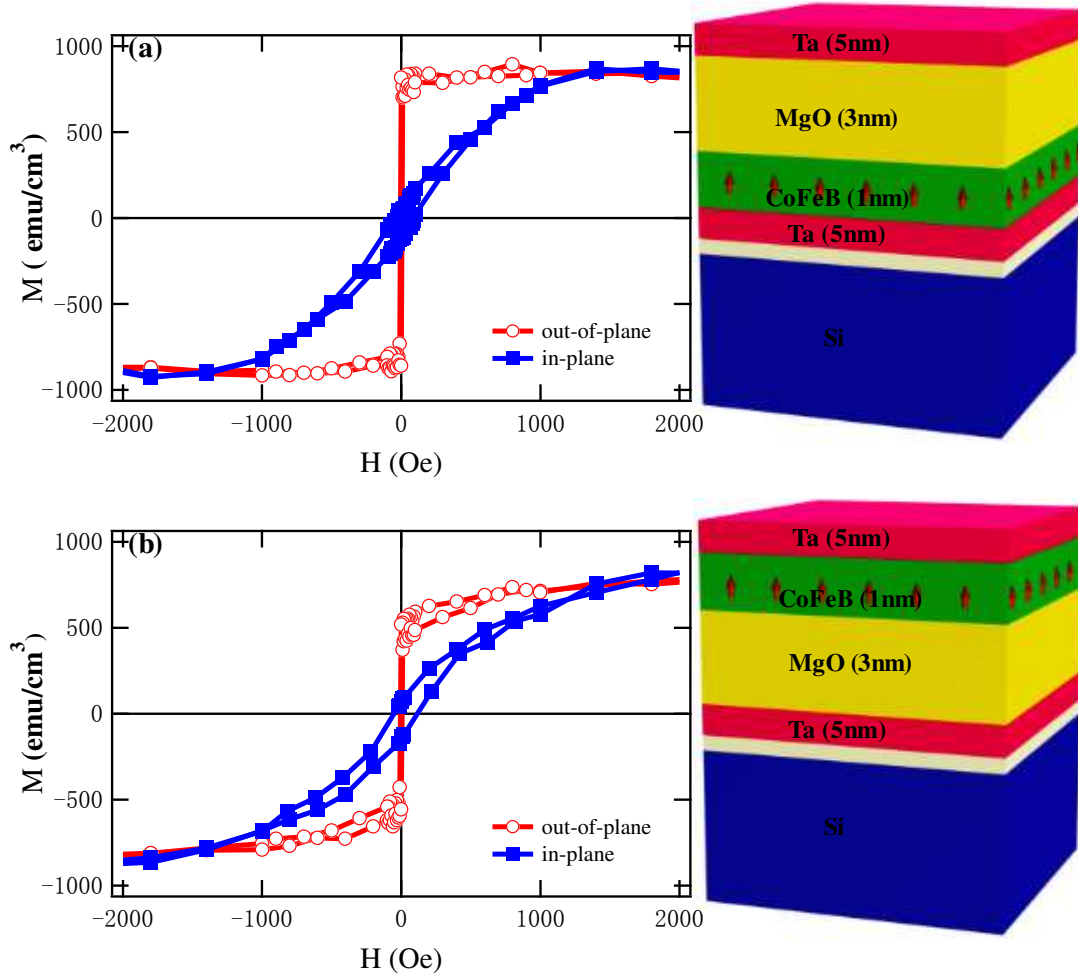
Fig. 1. (Color online) The M-H loops measured by VSM for (a) substrate/Ta/CoFeB (1nm)/MgO/Ta and (b) substrate/Ta/MgO/CoFeB (1nm)/Ta. The open circle shows the M-H loop with out-of-plane magnetic field, and the solid square presents the in-plane M-H loop.
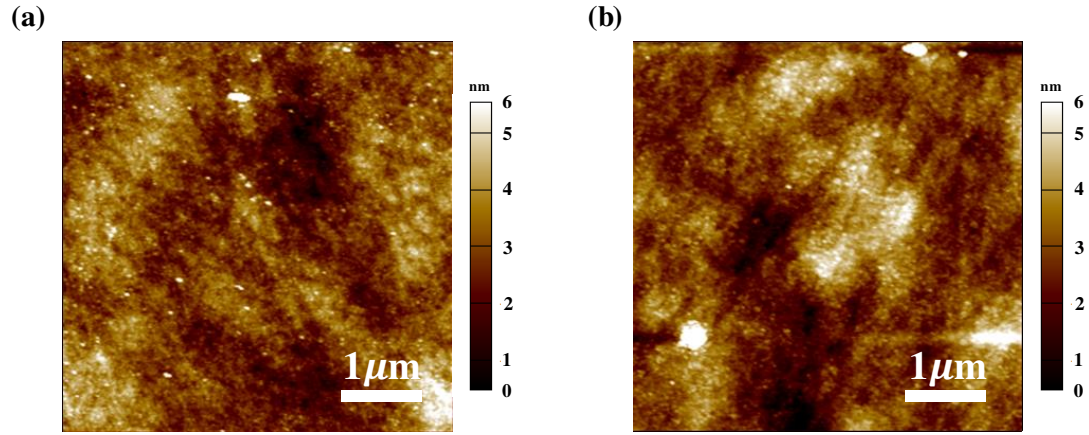
Fig. 2. (Color online) 2D AFM images measured on the surface of films with a structure of (a) substrate/Ta/CoFeB (1nm)/MgO/Ta, and (b) substrate/Ta/MgO/CoFeB (1nm)/Ta. The images correspond to a 5 μm×5 μm sample area.
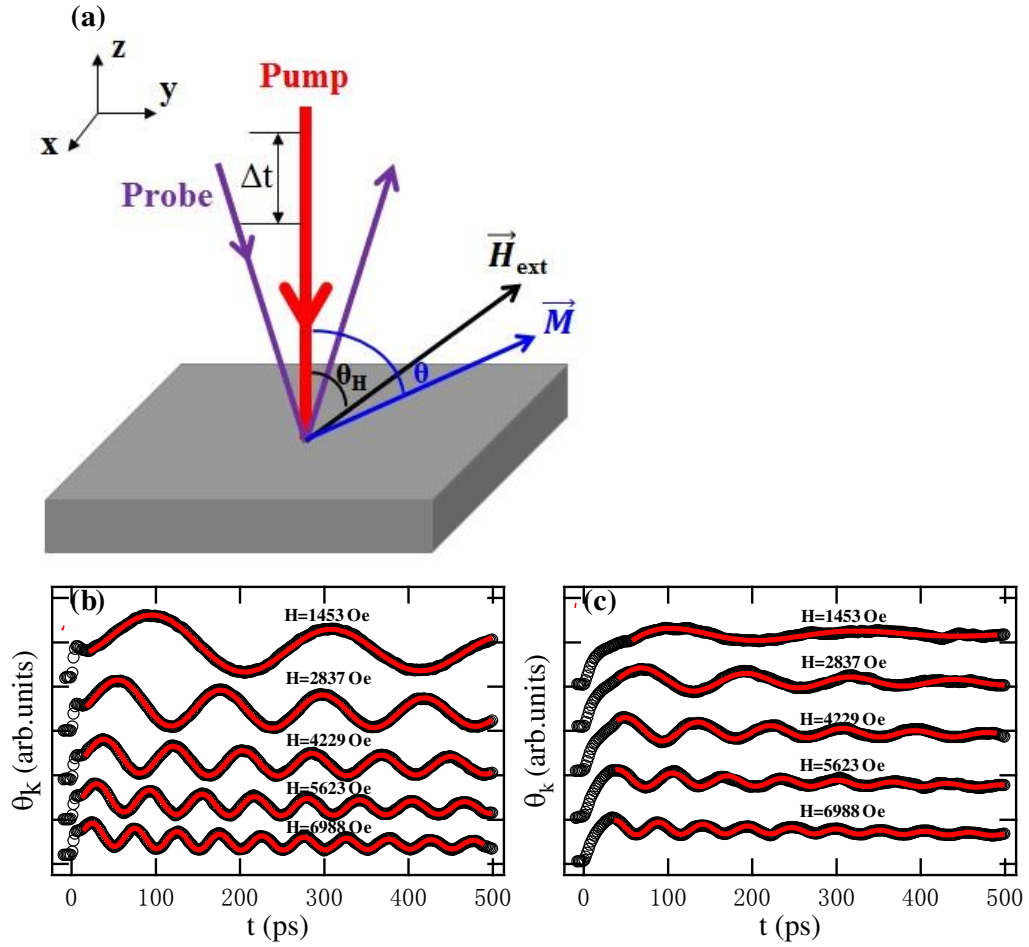
Fig. 3. (Color online) (a) Schematic of the TRMOKE measurements. Time-resolved Kerr rotation traces (solid circles) and fitting curves (red lines) for (b) substrate/Ta/CoFeB (1nm)/MgO/Ta and (c) substrate/Ta/MgO/CoFeB (1nm)/Ta films annealed at 300 ℃, which were measured by applying various external fields directed at 60° with respect to the film normal direction.
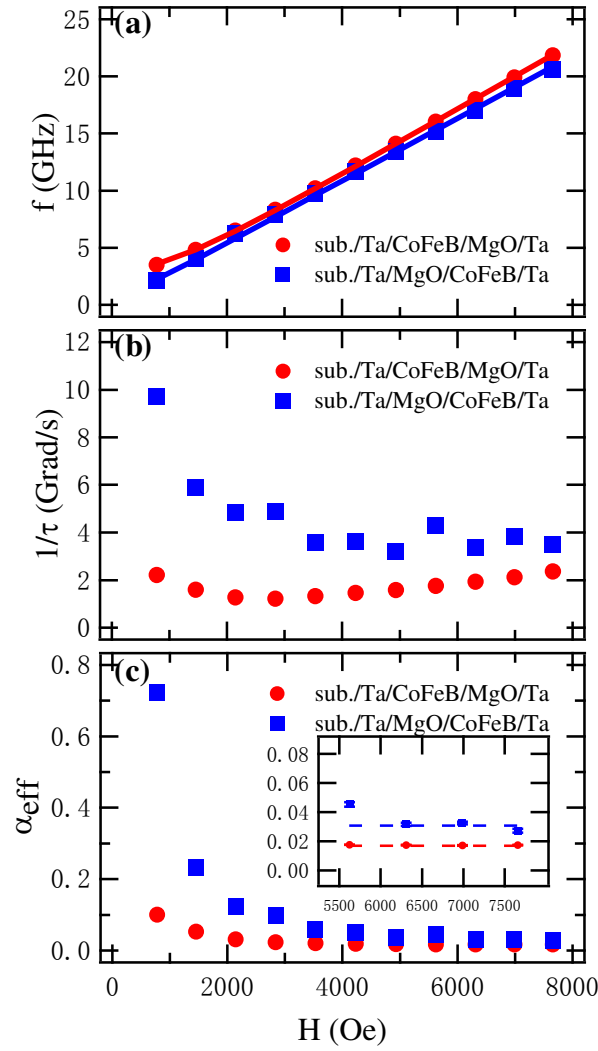
Fig. 4. (Color online) The magnetic field dependence of (a) the precession frequency f and (b) the inverse of relaxation lifetime $1/\tau$. The solid lines are the fitting lines. (c) The effective damping constant α_{eff} as a function of magnetic field. The inset in c) is an enlarged view in the vicinity of $H = 6500$ Oe and the dotted lines are fitted curves to the experimental data. Error bar denotes the fitting uncertainties.